

SCIENTIFIC REPORTS



OPEN

A Hiatus of the Greenhouse Effect

Jinjie Song, Yuan Wang & Jianping Tang

The rate at which the global average surface temperature is increasing has slowed down since the end of the last century. This study investigates whether this warming hiatus results from a change in the well-known greenhouse effect. Using long-term, reliable, and consistent observational data from the Earth's surface and the top of the atmosphere (TOA), two monthly gridded atmospheric and surface greenhouse effect parameters (G_a and G_s) are estimated to represent the radiative warming effects of the atmosphere and the surface in the infrared range from 1979 to 2014. The atmospheric and surface greenhouse effect over the tropical monsoon-prone regions is found to contribute substantially to the global total. Furthermore, the downward tendency of cloud activity leads to a greenhouse effect hiatus after the early 1990s, prior to the warming pause. Additionally, this pause in the greenhouse effect is mostly caused by the high number of La Niña events between 1991 and 2014. A strong La Niña indicates suppressed convection in the tropical central Pacific that reduces atmospheric water vapor content and cloud volume. This significantly weakened regional greenhouse effect offsets the enhanced warming influence in other places and decelerates the rising global greenhouse effect. This work suggests that the greenhouse effect hiatus can be served as an additional factor to cause the recent global warming slowdown.

Received: 17 February 2016
Accepted: 24 August 2016
Published: 12 September 2016

The rate at which the global average surface air temperature (T_s) increases has slowed down during the past few decades¹. This so-called hiatus, pause, or slowdown of global warming has inspired investigations into its potential causes worldwide^{1,2}. Although some researchers doubted the existence of a global warming hiatus because of coverage bias^{3,4}, artificial inconsistency⁵, and a change point analysis of instrumental T_s records⁶, it is now accepted that a recent warming deceleration can be clearly observed¹. There are two primary hypotheses to explain the recent slowdown of the upward trend in T_s ⁷. Both hypotheses attempt to explain the contradiction between the trendless T_s variation and the intensifying anthropogenic greenhouse effect resulting from the steadily increasing emission of greenhouse gases (GHGs). The first attributes the warming hiatus to external radiative forcings, such as decreasing solar irradiance⁸, increasing tropospheric and stratospheric aerosols⁹, reduced stratospheric water vapor¹⁰, and several small volcanic eruptions¹¹. The warming effect of increasing GHGs is largely cancelled out by the decreasing solar shortwave radiation received by the Earth's surface. The second considers the warming pause to be a result of internal oceanic and/or atmospheric decadal variabilities against the centennial warming trend¹², in which two leading theories are proposed. One asserts that the recent warming hiatus likely results from a La Niña-like state or a negative phase of Interdecadal Pacific Oscillation (IPO) associated with the cooling tropical Pacific sea surface temperature (SST) and the increasing Pacific trade winds^{12–26}. This theory is supported by the successful simulation of the warming hiatus by nudging the tropical Pacific SST or trade winds relative to observations^{14,17,19}. The other suggests that the warming hiatus is accompanied by increasing heat uptake in global deep oceans^{27–31}. This extra heat, which originates from a positive radiative imbalance at the top of the atmosphere (TOA), is reserved in the deep oceans instead of warming the Earth's skin^{32–36}. Note that both aforementioned hypotheses indeed include an enhancing greenhouse effect in which more heat is captured by the Earth–atmosphere system. The main difference between them is how this additional energy is prevented from warming the Earth's surface.

The variation of T_s is commonly influenced by changes in the greenhouse effect. In theory, an enhanced (reduced) greenhouse effect will accelerate (decelerate) the upward tendency of T_s . However, less discussion has addressed whether the Earth's greenhouse effect is intensified as GHGs increase from the observational perspective. A few studies have used satellite-based TOA radiation observations to detect changes related to the greenhouse effect^{37–41}. Harries *et al.*³⁸ found that more terrestrial heat is captured by several main GHGs (e.g., CO₂, CH₄, and O₃) in clear skies because the spectral brightness temperatures in their absorption bands used to measure the upwelling thermal energy were significantly reduced. However, their experimental evidence of an enhancing greenhouse effect was largely biased because the influences of water vapor and clouds, which contribute approximately 75% of the total effect, were not included⁴². In contrast, Raval and Ramanathan³⁷ employed a

School of Atmospheric Sciences, Nanjing University, China. Correspondence and requests for materials should be addressed to Y.W. (email: yuanasm@nju.edu.cn)

parameter (G_a) to quantify the magnitude of the atmospheric greenhouse effect including all potential contributors. G_a is the residual obtained by subtracting the TOA outgoing longwave radiation (OLR) from the surface upwelling longwave radiation (SULR). This parameter measures the vertically integrated greenhouse effect in the entire atmosphere and enters directly into the basic equations describing the climate. Furthermore, Cess and Udelhofen⁴³ reported a significant decreasing tendency of normalized G_a ($\Delta G_a = G_a/\text{SULR}$) for the 40°S to 40°N domain between 1985 and 1999 based on measurements of the TOA energy budget and Earth's surface temperature. They attributed this downward trend of the greenhouse effect to a notable reduction in cloud cover⁴³.

Whether the observational greenhouse effect is intensified during the warming hiatus period remains unclear. With the steady rise of anthropogenic GHG concentrations, does the heat trapped and then re-emitted to the surface by the atmosphere also increase? In addition, the change of the Earth's surface temperature has been shown down to be non-uniform in different regions and different sub-periods during recent decades⁴⁴. Does the greenhouse effect have some spatial or temporal characteristics similar to those in T_s ? Thus, the primary goal of this study is to investigate the spatiotemporal evolution of the greenhouse effect to better evaluate its potential impact. In this work, the monthly gridded G_a between 1979 and 2014 is estimated from the High-resolution Infrared Radiation Sounder (HIRS) OLR climate dataset⁴⁵ provided by the National Center for Environmental Information (NCEI) and the HadCRUT4 surface air temperature (T_s) dataset⁴⁶ provided by the Climatic Research Unit (CRU). The SULR is calculated using the blackbody radiation law ($\text{SULR} = \sigma T_s^4$, where σ is the Stefan–Boltzmann constant) of Raval and Ramanathan³⁷. The monthly gridded surface greenhouse effect parameter (G_s), which is defined as the downwelling longwave radiation (F_{\downarrow}) at the Earth's surface by Boer⁴⁷, is also obtained using a radiative transfer model from the National Aeronautics and Space Administration (NASA) Clouds and the Earth's Radiant Energy System (CERES) Energy Balanced And Filled (EBAF) product⁴⁸.

Results

The radiative warming effects of the atmosphere and the surface in the infrared range can be described by G_a and G_s ⁴⁷, whose climatological means are 158 W m^{-2} and 345 W m^{-2} , respectively, from 2003 to 2014. G_a represents the ability of the atmosphere to trap approximately 40% of the longwave radiation emitted by the Earth's surface (399 W m^{-2}). G_s indicates the energy sent by the atmosphere to the surface to heat the Earth. Nearly half of G_s comes from G_a , and the rest comprises the solar incidence, sensible and latent heat absorbed by the atmosphere⁴⁹. Figure 1 represents the spatial patterns of the estimated mean G_a and G_s between 2003 and 2014. Although G_a and G_s are both spatially inhomogeneous, they share similar spatial distributions. First, on average, both G_a and G_s decrease with increasing latitude. The zonal means of G_a (G_s) are 189 W m^{-2} (394 W m^{-2}) and 90 W m^{-2} (231 W m^{-2}) in the tropics (30°S–30°N) and polar zones (90°S–60°S and 60°N–90°N), respectively. The latitudinal patterns of G_a and G_s are mostly caused by the zonal distribution of the atmospheric water vapor content, which is the most important contributor to the greenhouse effect⁴². The wetter atmosphere at low latitudes thus absorbs more terrestrial radiation than the drier atmosphere at high latitudes. The surface condition is another important contributor to the G_s distribution. The wetter and warmer surface in the tropics provides greater latent and sensible heat to the atmosphere, which is included in G_s ⁴⁷. Second, because more atmospheric and surface moisture is found at sea than on land, on average, the oceanic G_a and G_s (162 W m^{-2} and 358 W m^{-2}) are slightly larger than the terrestrial values (148 W m^{-2} and 312 W m^{-2}). When the large proportion of oceans covering the Earth's surface is considered, the oceanic G_a (G_s) contributes more than three-quarters of the global total G_a (G_s). Moreover, nearly half of the global greenhouse effect is attributed to G_a (G_s) over the tropical oceans. Third, either G_a or G_s displays a meridional heterogeneity at the tropics. On the one hand, larger G_a and G_s (above 220 W m^{-2} and 420 W m^{-2} , respectively) are found in the Indo-West Pacific, Amazon and East Africa. This pattern coincides with the location of the tropical monsoons⁵⁰ that often deliver persistent convection. In the monsoon-prone areas, a stronger greenhouse effect is induced by the wetter and cloudier atmosphere and by the moist surface. On the other hand, the G_a over the East Pacific and East Atlantic is relatively low (below 180 W m^{-2}) because these areas are generally controlled by persistent subsidence and have dry and cloudless atmospheres.

Based on the climatological (2003–2014) means of G_a and G_s , the long-term variations of their anomalies (G_{aa} and G_{sa}) can be obtained (Fig. 2). Because of the shorter period of the CERES EBAF product, the areal averaged G_{sa} is represented only between 2003 and 2014 in Fig. 2 but shows no notable trend over the globe, sea or land. Thus, the surface greenhouse effect has not been strengthened in the last decade. The temporal variations of G_{sa} and G_{aa} are highly correlated over the globe, sea and land in 2003–2014, with all correlation coefficients above 0.40 and significant at the 0.01 level based on Student's t -test. By contrast, G_{aa} can be obtained from 1979 to 2014 because of the longer instrumental observations of T_s and OLR. The most obvious feature is that the decadal trends of the global averaged G_{aa} are not uniform throughout the period (Fig. 2a). In the 1980s, a significant increasing G_{aa} tendency exists with a linear estimate of $0.19 \text{ W m}^{-2} \text{ yr}^{-1}$. However, this uprising trend pauses starting in circa 1992, when G_{aa} begins to slightly decrease at a rate of $-0.01 \text{ W m}^{-2} \text{ yr}^{-1}$. This statistically non-significant trend indicates that the enhancing global atmospheric greenhouse effect is slowed down. Moreover, the atmospheric greenhouse effect hiatus can be found over both sea and land (Fig. 2b–c). Because the global total atmospheric greenhouse effect is largely controlled by the atmosphere over the oceans, the temporal variation of the averaged G_{aa} at sea is similar to the global value (Fig. 2b). The tendency of the averaged G_{aa} over the oceans also abruptly changes circa 1992. The oceanic G_{aa} exhibits a notable increasing trend with a rate of $0.21 \text{ W m}^{-2} \text{ yr}^{-1}$ in 1979–1991, whereas its rate of change ($-0.04 \text{ W m}^{-2} \text{ yr}^{-1}$) during 1992–2014 is not statistically significant. By contrast, although a sudden change in the G_{aa} tendency is observed overland, the breakpoint is approximately 5 years later than that of the oceanic G_{aa} (Fig. 2c). The terrestrial G_{aa} trends are $0.12 \text{ W m}^{-2} \text{ yr}^{-1}$ and $0.05 \text{ W m}^{-2} \text{ yr}^{-1}$ before and after 1997, respectively.

Because G_a is jointly determined by the longwave radiation at the surface and the TOA, the T_s and OLR evolutions are employed to discuss the formation of the global atmospheric greenhouse effect hiatus (Fig. S1). Here, the time period is divided into three 12-year subperiods (1979–1990, 1991–2002 and 2003–2014). The first break

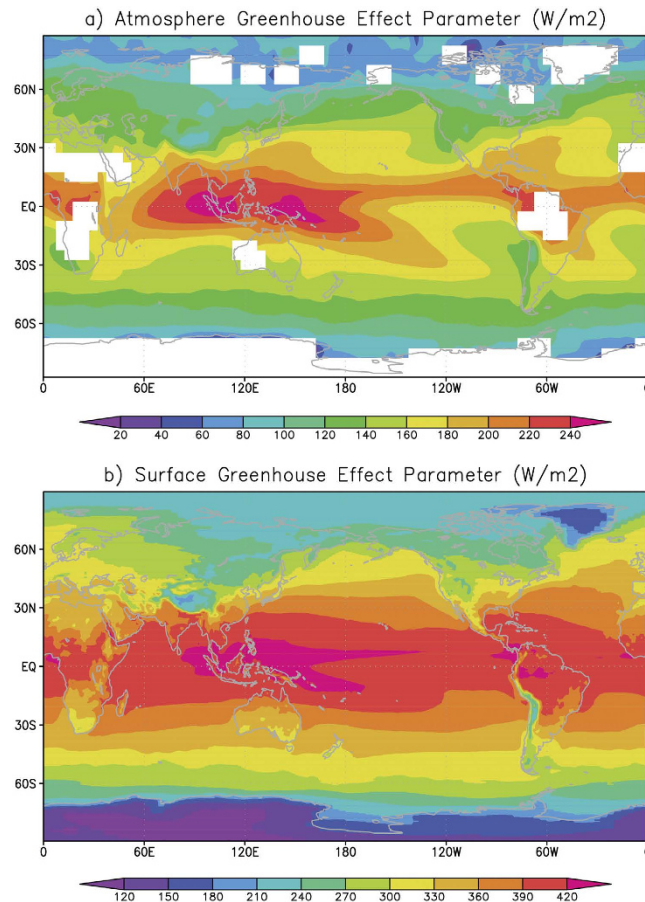


Figure 1. Spatial distributions of climatological averaged greenhouse effect parameter (G ; unit: W m^{-2}) on a 5° by 5° box between 2003 and 2014. (a,b) refer to the atmospheric and surface greenhouse effect parameters (G_a and G_s), respectively. The maps were generated by the Grid Analysis and Display System (GrADS; <http://www.opengrads.org/doc/wind32-v1/>) version 1.90-rc1.

point is used to separate the varying long-term global G_{aa} behavior in Fig. 2a. The second break point represents the beginning of the global warming pause because the increasing global averaged T_s tendency slowed down in the early 21st century¹⁵. In the first subperiod (1979–1990), the increasing T_s leads to a remarkable uprising trend in the global averaged SULR anomaly of $0.07 \text{ W m}^{-2} \text{ yr}^{-1}$, whereas the global averaged OLR anomaly exhibits a significant decreasing trend of $-0.10 \text{ W m}^{-2} \text{ yr}^{-1}$. Both of these behaviors enhance the atmospheric greenhouse effect, as indicated by an increase in G_{aa} . However, in the following subperiod, the rates of change of the SULR and OLR anomalies are both significantly positive. The former ($0.15 \text{ W m}^{-2} \text{ yr}^{-1}$) is comparable to the latter ($0.14 \text{ W m}^{-2} \text{ yr}^{-1}$). Therefore, their contributions to the atmospheric greenhouse effect nearly cancel each other out. As a result, an unchanged global averaged G_{aa} is shown during 1991–2002. In the last subperiod, the global averaged SULR anomaly remains trendless ($0.02 \text{ W m}^{-2} \text{ yr}^{-1}$) because T_s stops rising. Meanwhile, the long-term change of the global averaged OLR anomaly ($-0.01 \text{ W m}^{-2} \text{ yr}^{-1}$) is also not statistically significant. Thus, these two phenomena result in a trendless G_{aa} .

Furthermore, the trends of G_{aa} are spatially inhomogeneous during individual subperiods (Fig. 3). G_{aa} increases the most over the central North Pacific with a tendency of approximately $0.12 \text{ W m}^{-2} \text{ yr}^{-1}$ in 1979–1990 (Fig. 3a). Significant upward G_{aa} trends are also found at the tropical Atlantic and the high latitudes of Eurasia. By contrast, almost no regions exhibit a significant downward G_{aa} trend. This finding explains why the global averaged G_{aa} increases during this period. Similar to the previous period, an uprising G_{aa} trend is found over the central North Pacific from 1991 to 2002 with a reduced rate (Fig. 3b). Meanwhile, G_{aa} increases by substantially more in the western tropical Pacific, where the largest tendency ($0.18 \text{ W m}^{-2} \text{ yr}^{-1}$) is found, and in the central South Pacific. However, a remarkably decreasing G_{aa} trend ($-0.27 \text{ W m}^{-2} \text{ yr}^{-1}$) exists over the central tropical Pacific, indicating a weakened atmospheric greenhouse effect in this area, which largely offsets the warming effect in the aforementioned surrounding regions. As a result, a trendless global averaged G_{aa} is displayed between 1991 and 2002 (Fig. 2). During the latest subperiod (2003–2014), the spatial pattern of the change in G_{aa} is quite similar to that in 1991–2002, but the proportion of regions with significant G_{aa} tendencies is significantly reduced (Fig. 3c). Although the maximum upward and downward G_{aa} tendencies also appear over the western tropical Pacific and the central tropical Pacific, respectively, the increasing trend is nearly absent in the extratropics. Again, no significant trend of the global averaged G_{aa} is found from 2003 to 2014 (Fig. 2) because the enhanced warming

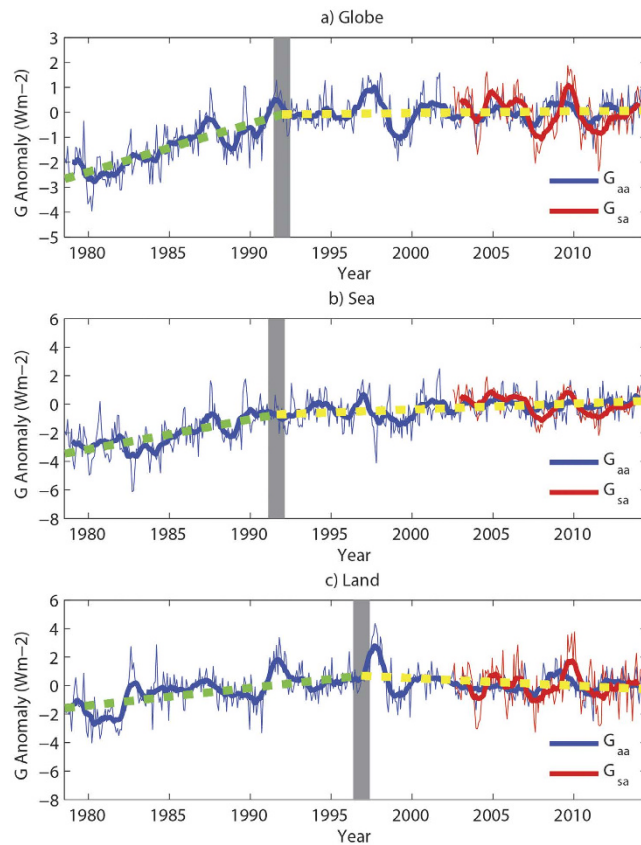


Figure 2. Monthly variations of the areal averaged atmospheric and surface greenhouse effect parameter anomalies (G_{aa} and G_{sa}) from 1979 to 2014 for the (a) globe, (b) sea and (c) land. G_{aa} and G_{sa} are represented by blue and red lines, respectively. Thin and thick solid lines indicate the monthly and 12-month moving averaged series, respectively. Vertical, thick, gray lines represent the break points of trends using the break function regression (see Methods). Green and yellow dashed lines refer to linear trend lines before and after the break points, respectively. The figure was plotted using MATLAB software.

effect over the western tropical Pacific is largely counteracted by the weakened warming influence on the central tropical Pacific.

The results above indicate that the notably downward G_{aa} tendency over the central tropical Pacific indeed plays an important role in inducing the greenhouse effect hiatus since the 1990s. What causes this decreasing G_{aa} ? The variation of the greenhouse effect is substantially influenced by its contributors, including water vapor, clouds, and GHGs⁴². GHG concentrations have risen steadily during recent decades¹. The variations of metrics related to the other two contributors are given in Fig. 4a and are based on the CERES-EBAF products between 2003 and 2014. The total column precipitable water (TCPW) anomaly significantly increases at a rate of 0.44 cm yr^{-1} . However, the cloud area fraction (CAF) anomaly is reduced by $-0.60\% \text{ yr}^{-1}$, which is consistent with the decreasing cloud activity described in previous publications⁵¹. Therefore, although the greenhouse effect can be enhanced by increasing GHGs and water vapor in the atmosphere, it can be weakened by decreasing clouds. If these two actions offset each other, a hiatus of the global greenhouse effect will result. To confirm this, the variations of G_{aa} and G_{sa} in all-sky conditions are compared with those in clear-sky conditions in Fig. 4b,c. The clear-sky atmospheric and surface greenhouse effect parameters increase significantly at rates of $0.22 \text{ W m}^{-2} \text{ yr}^{-1}$ and $0.19 \text{ W m}^{-2} \text{ yr}^{-1}$, respectively. However, the atmospheric and surface greenhouse effect parameters both become trendless when clouds are considered. Moreover, the spatial pattern of the CAF anomaly trend (Fig. S2) is very similar to that of the G_{aa} trend (Fig. 3c) during 2003–2014. Cloud activity becomes less active over the central tropical Pacific, whereas it is enhanced over the western and eastern tropical Pacific. Overall, the downward tendency of clouds is the dominant contributor to the greenhouse effect hiatus.

Interestingly, the spatial structure exhibits a seesaw pattern between the central tropical Pacific and the western/eastern tropical Pacific in both the G_{aa} tendency and CAF anomaly trend from 2003 to 2014 (Fig. 3c, Fig. S2). This pattern is similar to that of the composited SST anomaly in strong La Niña events^{51,52}. Further, the decreasing G_{aa} trend can result from La Niña events occurring more frequently in the last two decades. The Niño 3.4 SST anomaly shows no significant tendency between 1979 and 1990, whereas it decreases remarkably after 1990 at a rate of $-0.028 \text{ °C yr}^{-1}$ (Fig. S3). Notably, the first half of the downward Niño 3.4 SST anomaly trend is much larger than the second half. This finding is consistent with a stronger decreasing G_{aa} trend over the central tropical Pacific during 1991–2002 (Fig. 3). Strong La Niña events are associated with strong anomalous cooling and

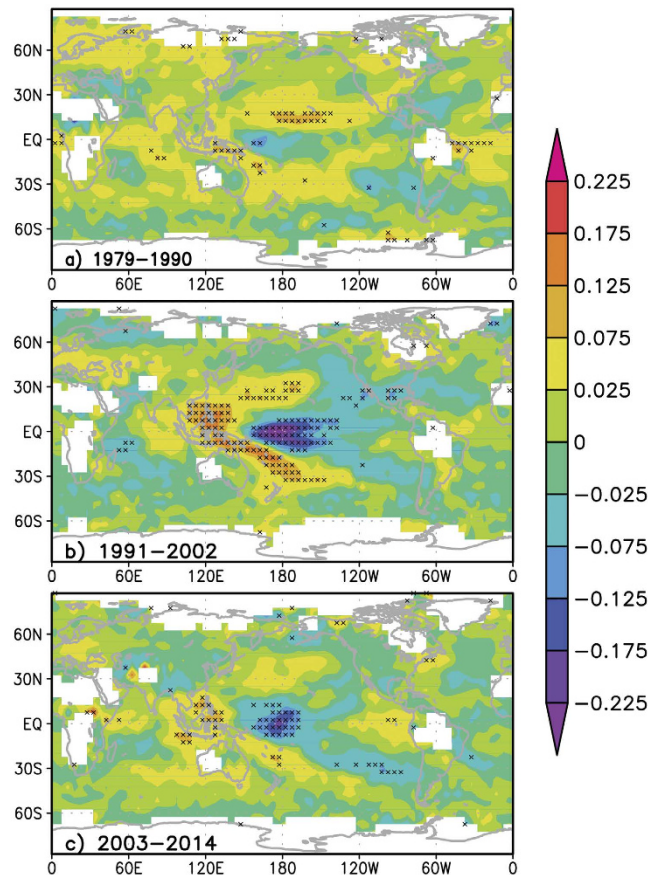


Figure 3. Spatial structures of the atmospheric greenhouse effect parameter anomaly (G_{aa}) trend on a 5° by 5° box using the least-squares approach during three subperiods: (a) 1979–1990, (b) 1991–2002, and (c) 2003–2004. Regions with a significant tendency (at the 0.05 confidence level based on the F -test) are crossed. Maps were generated by GrADS (<http://www.opengrads.org/doc/wind32-v1/>) version 1.90-rc1.

suppressed convection in the central tropical Pacific^{52,53}. Therefore, this La Niña-related phenomenon can reduce atmospheric water vapor content and cloud volume and further weaken the greenhouse effect over the central tropical Pacific.

Discussion

The Earth's environment is suitable for life because of the greenhouse effect. Our planet has become increasingly warm since the Industrial Revolution because of the increased GHG emissions, which greatly enhance the greenhouse effect. However, the uprising rate of the Earth's T_s has slowed down in recent years. Whether this global warming pause is accompanied by a hiatus of the greenhouse effect is investigated in this study. The regional and global greenhouse effects are quantitatively estimated from reliable T_s observations and consistent OLR satellite products in 1979–2014. Although the change of OLR is theoretically in accordance with that of the tropospheric temperature according to the Stefan–Boltzmann Law, in reality, their relationship is more complex⁵⁴. Different tendencies of OLR and T_s can be seen in different periods, leading to an atmospheric and surface greenhouse effect hiatus since the early 1990s. This pause exists not only over the oceans but also over the continents. Further analysis indicates that this hiatus is very likely a result of the occurrence of more La Niña events after 1992. In the strong La Niña phase, both the atmospheric water vapor and the cloud volume are greatly reduced over the central tropical Pacific, amplifying the regional weakened greenhouse effect. Therefore, G_{aa} decreases significantly during 1992–2014 over the central tropical Pacific, which offsets the upward G_{aa} tendencies occurring elsewhere.

Interestingly, the atmospheric greenhouse effect hiatus occurs ahead of the global warming slowdown. Does the former lead to the latter? To answer this question, the cross-correlation coefficients between the G_{aa} and the T_s anomaly (T_a) on different timescales are given in Fig. 5. The simultaneous correlations are largest on the whole timescales, which likely indicates a positive feedback between T_s and the greenhouse effect. By contrast, the secondary maximum consistently appears with a lag of approximately 5 years. Moreover, larger and more significant correlations are found when G_{aa} leads T_a than when G_{aa} trails T_a . Thus, the variability of T_a may depend on the foregoing change of G_{aa} . In conclusion, the pause of the greenhouse effect since the 1990s may be one of the reasons for the global warming hiatus starting in the early 2000s.

It is well accepted that the recent global warming slowdown is attributable to the joint effect of internal natural variability and external forcing¹². In general, the warming hiatus is mainly driven by internal variability such as a negative phase of the IPO as well as a more La Niña-dominated state, with a minor external contribution⁸.

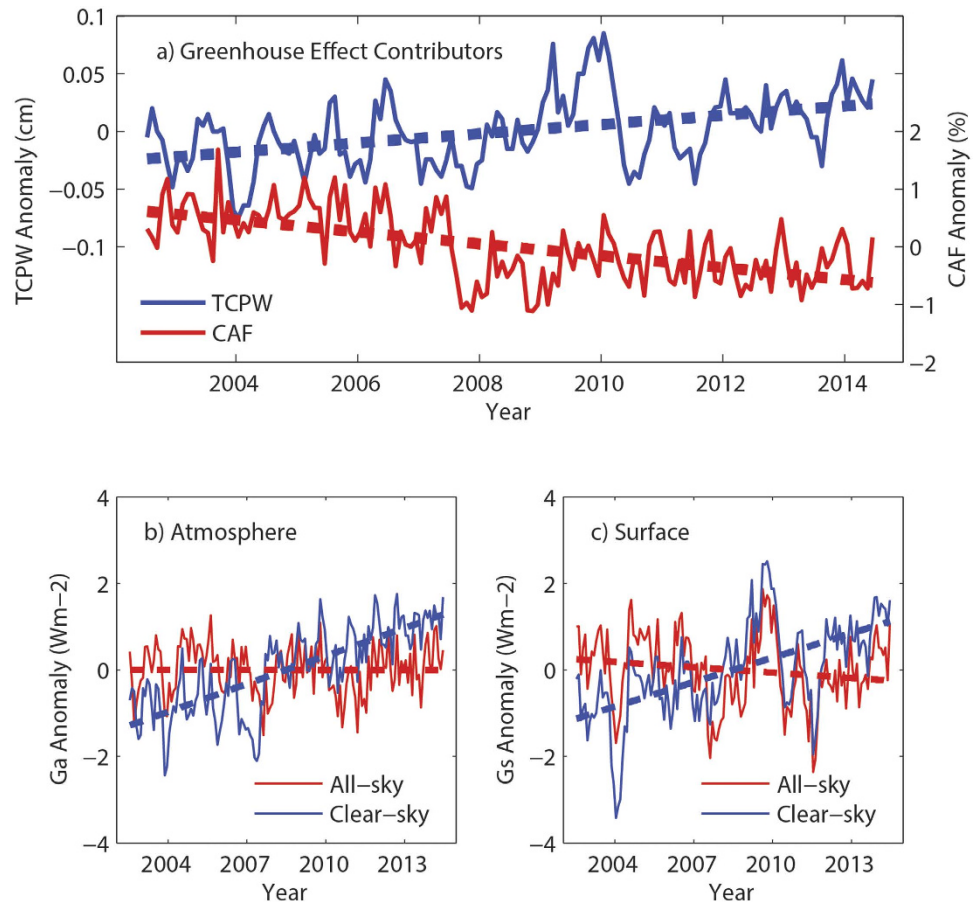


Figure 4. (a) Monthly variations of the global averaged TCPW (unit: cm) and CAF (unit: %) anomalies between 2003 and 2014. Dashed lines are the linear trend lines obtained by the least squares method. (b) Monthly variations of the atmospheric greenhouse effect parameter anomaly (G_{aa} ; unit: $W m^{-2}$) from 2003 to 2014 for all-sky (red lines) and clear-sky (blue lines) conditions. Dashed lines are the linear trend lines obtained by the least squares method. (c) Same as (b) but for the surface greenhouse effect parameter anomaly (G_{sa} ; unit: $W m^{-2}$). The figure was plotted using MATLAB software.

However, a recent study found that the phase of the IPO could be modulated by anthropogenic aerosols, in which case external forcing was attributed to be the primary factor decelerating global warming⁵⁵. By contrast, this study is not focused on the potential causes of different IPO or ENSO phases. Instead, we represent an alternative pathway of internal variability driving the warming slowdown. A La Niña-like state suppresses convection in the tropical central Pacific and concomitantly reduces cloud coverage. Consequently, a zero-trend greenhouse effect is achieved under the balance of its primary contributors (e.g. water vapor, clouds, and GHGs). Finally, the hiatus of the greenhouse effect-driven warming leads to the recent global warming slowdown, in which the atmosphere traps (emits) near constant heat from (to) the surface.

Methods

Surface temperature (T_s). The global monthly absolute T_s records are derived by combining the temperature anomaly and the base temperature with a spatial resolution of $5^\circ\text{long} \times 5^\circ\text{lat}$ from 1979 to 2014. The combined land and marine T_s anomalies relative to the base period 1961–1990 are provided by the joint work of the CRU of the University of East Anglia and the Hadley Centre of the UK Met Office⁵⁶. The corresponding absolute T_s for the aforementioned base period is given by Jones *et al.*⁵⁷.

HIRS OLR. The global monthly product of OLR at the TOA is obtained from the Climate Data Record (CDR) program organized by the National Oceanic and Atmospheric Administration (NOAA) in 1979–2014⁴⁵. These consistent, long-term OLR records are derived using the radiance observations from the HIRS onboard the NOAA Television Infrared Observation Satellite (TIROS)-N series and the Eumetsat MetOp-A satellites. The original gridded $2.5^\circ \times 2.5^\circ$ OLR data are interpolated on a 5° by 5° box.

NASA CERES EBAF satellite products. The monthly OLR and surface downwelling longwave radiation in all-sky and clear-sky conditions between 2003 and 2014 are provided by the NASA CERES EBAF product⁴⁸.

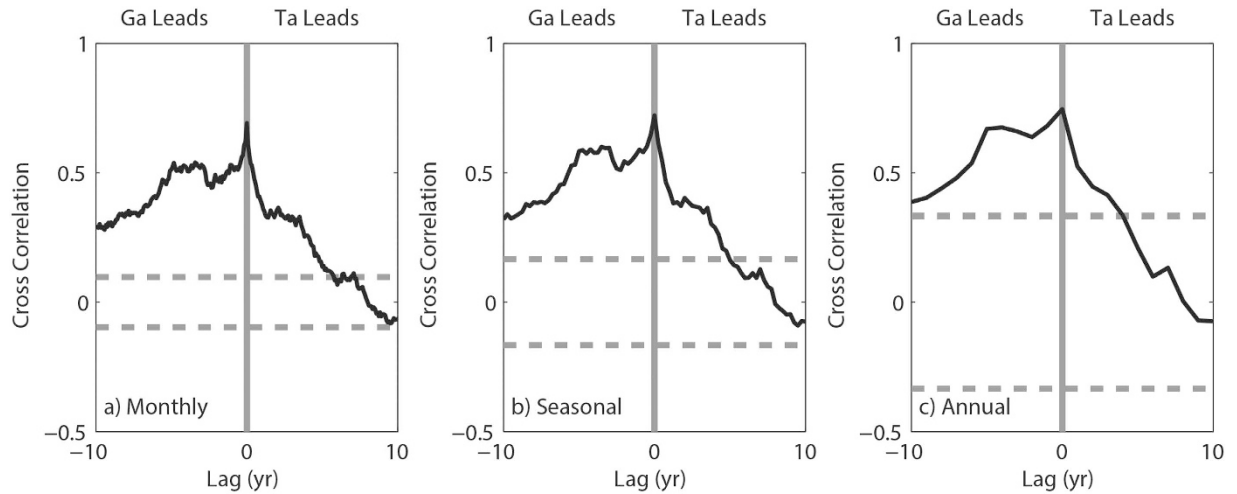


Figure 5. Cross-correlation coefficients between the global averaged atmospheric greenhouse effect parameter anomaly (G_{aa}) and the global mean surface temperature anomaly (T_a) on three time scales: (a) monthly, (b) seasonal and (c) annual. The horizontal dashed line refers to the significance at the 0.05 level. Positive (negative) lags indicate that T_a leads (trails) G_{aa} . The figure was plotted using MATLAB software.

The monthly CAF and TCPW are from the same product. The original gridded $1^\circ \times 1^\circ$ data are all interpolated on a 5° by 5° box.

Atmospheric greenhouse effect parameter (G_a). The monthly G_a values are calculated by $G_a = \sigma T_s^4 - \text{OLR}$ on each 5° by 5° grid⁴², where σ is the Stefan-Boltzmann constant ($5.67 \times 10^{-8} \text{ W m}^{-2} \text{ K}^{-4}$). G_a represents the difference between the heat emitted by the Earth's surface and the longwave radiation escaping from the TOA. The former energy is estimated based on the assumption of blackbody radiation; thus, the emissivity (ϵ) is close to one for every underlying surface. This assumption is confirmed by the global surface emissivity map (Fig. S4) derived using the NASA CERES EBAF products⁴⁸.

Surface greenhouse effect parameter (G_s). The monthly G_s values are defined by $G_s = F_\downarrow$ on individual 5° by 5° grids, where F_\downarrow refers to the downwelling longwave radiation at the Earth's surface.

Break function regression. This procedure objectively estimates the change point of different tendencies in time series by combining a weighted least-squares criterion with a brute-force search and the linear trends before and after the discontinuity⁵⁸. It is similar to the piecewise linear regression method with one change point reported in other publications^{6,59,60}. The break function model for time series $X(T)$, written as

$$x(T) = \begin{cases} x_1 + \frac{x_2 - x_1}{t_2 - t_1}(T - t_1) & \text{for } T \leq t_2 \\ x_2 + \frac{x_3 - x_2}{t_3 - t_2}(T - t_2) & \text{for } T > t_2 \end{cases} + \epsilon(T), \quad (1)$$

has four parameters: x_1 , x_2 , x_3 and t_2 . The former three can be estimated using the least-squares approach when t_2 is fixed. The break point t_2 is determined by maximizing the explained variance. The trends before and after the break point are determined as $(x_2 - x_1)/(t_2 - t_1)$ and $(x_3 - x_2)/(t_3 - t_2)$, respectively.

Trend analysis. The time series trend is estimated by the least squares method. In this study, the tendency is considered significant when it passes the F -test at the 0.05 level.

References

1. Fyfe, J. *et al.* Making sense of the early 2000s warming slowdown. *Nature Climate Change* **6**, 224–228 (2016).
2. Hawkins, E., T. Edwards & D. McNeill. Pause for thought. *Nature Climate Change*, **4**, 154–156 (2014).
3. Cowtan, K. & R. Way. Coverage bias in the HadCRUT4 temperature series and its impact on recent temperature trends. *Q. J. R. Meteorol. Soc.* **140**, 1935–1944 (2014).
4. Lewandowsky, S., J. Risbey & N. Oreskes. On the definition and identifiability of the alleged “hiatus” in global warming. *Sci. Rep.* **5**, 16784 (2015).
5. Karl, T. *et al.* Possible artifacts of data biases in the recent global surface warming hiatus. *Science* **348**, 1469–1472 (2015).
6. Cahill, N., S. Rahmstorf & A. Parnell. Change points of global temperature. *Environ. Res. Lett.* **10**, 084002 (2015).
7. Trenberth, K. Has there been a hiatus? *Science* **349**, 691–692 (2015).
8. Huber, M. & R. Knutti. Natural variability, radiative forcing and climate response in the recent hiatus reconciled. *Nature Geoscience* **7**, 651–656 (2014).
9. Kaufmann, R., H. Kauppi, M. Mann & J. Stock. Reconciling anthropogenic climate change with observed temperature 1998–2008. *Proc. Natl. Acad. Sci.* **108**, 11790–11793 (2011).

10. Solomon, S. *et al.* Contributions of stratospheric water vapor to decadal changes in the rate of global warming. *Science* **327**, 1219–1223 (2010).
11. Santer, B. *et al.* Volcanic contribution to decadal changes in tropospheric temperature. *Nature Geoscience* **7**, 185–189 (2014).
12. Liu, W. *et al.* Tracking ocean heat uptake during the surface warming hiatus. *Nature Communications* **7**, 10926 (2016).
13. Meehl, G. *et al.* Externally forced and internally generated decadal climate variability associated with the Interdecadal Pacific Oscillation. *J. Climate* **26**, 7298–7310 (2013).
14. Kosaka, Y. & S. Xie. Recent global-warming hiatus tied to equatorial Pacific surface cooling. *Nature* **501**, 403–407 (2013).
15. Watanabe, M. *et al.* Strengthening of ocean heat uptake efficiency associated with the recent climate hiatus. *Geophys. Res. Lett.* **40**, 3175–3179 (2013).
16. Trenberth, K. & J. Fasullo. An apparent hiatus in global warming? *Earth's Future* **1**, 19–32 (2013).
17. England, M. *et al.* Recent intensification of wind-driven circulation in the Pacific and the ongoing warming hiatus. *Nature Climate Change* **4**, 222–227 (2014).
18. Trenberth, K., J. Fasullo, G. Branstator & A. Phillips. Seasonal aspects of the recent pause in surface warming. *Nature Climate Change* **4**, 911–916 (2014).
19. Watanabe, M., H. Shiogama, H. Tatebe, M. Hayashi, M. Ishii & M. Kimoto. Contribution of natural decadal variability to global warming acceleration and hiatus. *Nature Climate Change*, **4**, 893–897 (2014).
20. Meehl, G., H. Teng & J. Arblaster. Climate model simulations of the observed early-2000s hiatus of global warming. *Nature Climate Change* **4**, 898–902 (2014).
21. Drijfhout, S. *et al.* Surface warming hiatus caused by increased heat uptake across multiple ocean basins. *Geophys. Res. Lett.*, **41**, 7868–7874 (2014).
22. Dai, A., J. Fyfe, S. Xie & X. Dai. Decadal modulation of global surface temperature by internal climate variability. *Nature Climate Change* **5**, 555–559 (2015).
23. Steinman, B., M. Mann & S. Miller. Atlantic and Pacific multidecadal oscillations and Northern Hemisphere temperatures. *Science* **347**, 988–991 (2015).
24. Nieves, V., J. Willis & W. Patzert. Recent hiatus caused by decadal shift in Indo-Pacific heating. *Science* **349**, 532–535 (2015).
25. Xie, S., Y. Kosaka & Y. Okumura. Distinct energy budgets for anthropogenic and natural changes during global warming hiatus. *Nature Geosciences*, doi: 10.1038/ngeo2581 (2015).
26. Takahashi, C. & M. Watanabe. Pacific trade winds accelerated by aerosol forcing over the past two decades. *Nature Climate Change* (2016).
27. Barnett, T. *et al.* Penetration of the human-induced warming into the world's oceans. *Science* **209**, 284–287 (2005).
28. Palmer, M. *et al.* A new perspective on warming of the global oceans. *Geophys. Res. Lett.* **36**, L20709 (2009).
29. Gleckler, P. *et al.* Human-induced global ocean warming on multidecadal timescales. *Nature Climate Change* **2**, 524–529 (2012).
30. Pierce, D. *et al.* The fingerprint of human-induced changes in the ocean's salinity and temperature fields. *Geophys. Res. Lett.* **39**, L21704 (2012).
31. Balmaseda, M., K. Trenberth & E. Kallen. Distinctive climate signals in reanalysis of global ocean heat content. *Geophys. Res. Lett.* **40**, 1754–1759 (2013).
32. Purkey, S. & G. Johnson. Warming of global abyssal and deep Southern Ocean waters between the 1990s and 2000s: contributions to global heat and sea level budgets. *J. Climate* **23**, 6336–6351 (2010).
33. Loeb, N. *et al.* Observed changes in top-of-the-atmosphere radiation and upper-ocean heating consistent with uncertainty. *Nature Geoscience* **5**, 110–113 (2012).
34. Meehl, G., J. Arblaster, J. Fasullo, A. Hu & K. Trenberth. Model-based evidence of deep-ocean heat uptake during surface-temperature hiatus periods. *Nature Climate Change* **1**, 360–364 (2011).
35. Chen, X. & K. Tung. Varying planetary heat sink led to global-warming slowdown and acceleration. *Science* **345**, 897–903 (2014).
36. Lee, S., W. Park, M. Baringer, A. Gordon, B. Huber & Y. Liu. Pacific origin of the abrupt increase in Indian Ocean heat content during the warming hiatus. *Nature Geoscience* **8**, 445–449 (2015).
37. Raval, A. & V. Ramanathan. Observational determination of the greenhouse effect. *Nature*, **342**, 758–761 (1989).
38. Harries, J., H. Brindley, P. Sahoo & R. Bantges. Increases in greenhouse forcing inferred from the outgoing longwave radiation spectra of the Earth in 1970 and 1997. *Nature* **410**, 355–357 (2001).
39. Philippona, R., B. Durr, C. Marty, A. Ohmura & M. Wild. Radiative forcing - measured at Earth's surface - corroborate the increasing greenhouse effect. *Geophys. Res. Lett.* **31**, L03202 (2004).
40. Timofeev, N. Greenhouse effect of the atmosphere and its influence on Earth's climate (satellite data). *Physical Oceanography* **16**, 322–336 (2006).
41. Gastineau, G., B. Soden, D. Jackson & C. O'Dell. Satellite-Based Reconstruction of the Tropical Oceanic Clear-Sky Outgoing Longwave Radiation and Comparison with Climate Models. *J. Climate* **27**, 941–957 (2014).
42. Schmidt, G., R. Ruedy, R. Miller & A. Lacis. The attribution of the present-day total greenhouse effect. *J. Geophys. Res.* **115**, D20106 (2010).
43. Cess, R. & P. Udelhofen. Climate change during 1985–1999: cloud interactions determined from satellite measurements. *Geophys. Res. Lett.* **30**, 1019 (2003).
44. Ji, F., Z. Wu, J. Huang & E. Chassignet. Evolution of land surface air temperature trend. *Nature Climate Change* **4**, 462–466 (2014).
45. Lee, H., A. Gruber, R. Ellingson & I. Laszlo. Development of the HIRS Outgoing Longwave Radiation climate data set. *J. Atmos. Ocean. Tech.* **24**, 2029–2047 (2007).
46. Kennedy, J., N. Rayner, R. Smith, M. Saunby & D. Parker. Reassessing biases and other uncertainties in sea-surface temperature observations measured *in situ* since 1850 part 2: biases and homogenisation. *J. Geophys. Res.* **116**, D14104 (2011).
47. Boer, G. Climate Change and the regulation of the surface moisture and energy budgets. *Clim. Dyn.* **8**, 225–239 (1993).
48. Wielicki, B., B. Barkstrom, E. Harrison, R. Lee III, G. Smith & J. Cooper. Clouds and the Earth's radiant energy system (CERES): an Earth observing system experiment. *Bull. Amer. Meteor. Soc.* **77**, 853–868 (1996).
49. Trenberth, K., J. Fasullo & J. Kiehl. Earth's global energy budget. *Bull. Amer. Meteor. Soc.* **90**, 311–323 (2009).
50. McKnight, T. & D. Hess. "Climate Zones and Types". *Physical Geography: A Landscape Appreciation* (Prentice Hall, 2000).
51. Herman, J. *et al.* A net decrease in the Earth's cloud, aerosol, and surface 340 nm reflectivity during the past 33 yr (1979–2011). *Atmos. Chem. Phys.* **13**, 8505–8524 (2013).
52. Takahashi, K. *et al.* ENSO regimes: reinterpreting the canonical and Modoki El Niño. *Geophys. Res. Lett.* **38**, L10704 (2011).
53. Dommenget, D., T. Bayr & C. Frauen. Analysis of the non-linearity in the pattern and time evolution of El Niño southern oscillation. *Clim. Dyn.* **40**, 2825–2847.
54. Von Schuckmann, K. *et al.* An imperative to monitor Earth's energy imbalance. *Nature Climate Change* **6**, 138–144 (2016).
55. Smith, D. *et al.* Role of volcanic and anthropogenic aerosols in the recent global surface warming slowdown. *Nature Climate Change* **6**, 1–6 (2016).
56. Morice, C. *et al.* Quantifying uncertainties in global and regional temperature change using an ensemble of observational estimates: the HadCRUT4 data set. *J. Geophys. Res.* **117**, D08101 (2012).
57. Jones, P., M. New, D. Parker, S. Martin & I. Rigor. Surface air temperature and its variations over the last 150 years. *Reviews of Geophysics* **37**, 173–199 (1999).

58. Mudelsee, M. Break function regression: a tool for quantifying trend changes in climate time series. *Eur. Phys. J. Special Topics* **174**, 49–63 (2009).
59. Ying, L., Z. Shen & S. Piao. The recent hiatus in global warming of the land surface: scale-dependent breakpoint occurrences in space and time. *Geophys. Res. Lett.* **42**, 6471–6478 (2015).
60. Werner, R. *et al.* Study of structural break points in global and hemispheric temperature series by piecewise regression. *Advances in Space Research* **56**, 2323–2334 (2015).

Acknowledgements

This work was jointly funded by the National Grand Fundamental Research 973 Program of China (2015CB452800) and the National Science Foundation of China (grant 41375075). We would like to thank Dr. Hai-Tien Lee for suggestions related to the HIRS OLR data set. We would like to thank Dr. Phil Klotzbach at Colorado State University for improving the language. We wish to express our sincere thanks to the anonymous reviewers for their helpful comments on an earlier manuscript.

Author Contributions

J.S. performed data analysis and wrote the manuscript. Y.W. proposed the original idea and set up the structure of this article. J.T. prepared the data and computed other parameters. All the authors reviewed the manuscript.

Additional Information

Supplementary information accompanies this paper at <http://www.nature.com/srep>

Competing financial interests: The authors declare no competing financial interests.

How to cite this article: Song, J. *et al.* A Hiatus of the Greenhouse Effect. *Sci. Rep.* **6**, 33315; doi: 10.1038/srep33315 (2016).



This work is licensed under a Creative Commons Attribution 4.0 International License. The images or other third party material in this article are included in the article's Creative Commons license, unless indicated otherwise in the credit line; if the material is not included under the Creative Commons license, users will need to obtain permission from the license holder to reproduce the material. To view a copy of this license, visit <http://creativecommons.org/licenses/by/4.0/>

© The Author(s) 2016